Journal of Alloys and Compounds 489 (2010) 424–428

Contents lists available at ScienceDirect

Journal of Alloys and Compounds

journal homepage: www.elsevier.com/locate/jallcom

Microstructure and mechanical properties of ultrafine-grained *fcc*/*hcp* cobalt processed by a bottom-up approach

F. Fellah[a], G. Dirras[a,*], J. Gubicza[b], F. Schoenstein[a], N. Jouini[a], S.M. Cherif[a], C. Gatel[c], J. Douin[c]

[a] *LPMTM, CNRS, UPR 9001, Université Paris 13, 99 Avenue Jean-Baptiste Clément, FR-93430 Villetaneuse, France*
[b] *Department of Materials Physics, Eötvös Loránd University, Budapest, P.O.B. 32, H-1518, Hungary*
[c] *CEMES – CNRS, 29 rue Jeanne Marvig, BP 94347, FR-31055 Toulouse Cedex, France*

ARTICLE INFO

Article history:
Received 27 July 2009
Received in revised form
23 September 2009
Accepted 24 September 2009
Available online 4 October 2009

Keywords:
Powder metallurgy
Sol–gel processes
Mechanical properties
Microstructure
Transmission electron microscopy (TEM)
X-ray diffraction

ABSTRACT

Bulk Co samples having a mean grain size of ~300 nm were processed by hot isostatic pressing of a high purity Co nanopowder synthesized by *chimie douce*. The grain interior exhibited a highly faulted nanoscale lamellar microstructure comprising an intricate mixture of face-centered cubic, hexagonal close-packed phases and nanotwins. Room temperature compression tests carried out at a strain rate of $\sim 2 \times 10^{-4}\ s^{-1}$ revealed a yield stress of ~1 GPa, a strain to rupture of ~5%. During straining it was found that the hexagonal close-packed phase content increased from 55% to 65% suggesting a deformation mechanism based on stress-assisted face-centered cubic to hexagonal close-packed phase transformation. In addition, an apparent activation volume of $\sim 3b^3$ was computed which indicates that the deformation mechanism was controlled by dislocation nucleation from the numerous boundaries. Nonetheless, in such an intricate microstructure, the overall mechanical properties are discussed in term of a complex interplay between lattice dislocation plasticity, transformation-induced plasticity and possibly twin-induced plasticity.
© 2009 Elsevier B.V. All rights reserved.

1. Introduction

The room temperature (RT) properties of metallic materials, such as their mechanical or physical properties change with the microstructure, especially with the grain size of polycrystalline aggregates. It is well known that for most metals and alloys, the yield strength increases with decreasing grain size according to the Hall-Petch law (HPL), which predicts that the yield strength increases linearly with the inverse square root of the grain size [1,2]. Many studies have shown that the HPL holds true to roughly 20–10 nm [3,4]. Below this grain size scale, the HPL breaks down and the flow stress decreases with decreasing grain size [5] due to the fact that within this regime, intragranular dislocation sources are unlikely to be active. Indeed, for such a small grain size, grain boundary-related processes predominate.

Macroscopically, it is observed that the high flow stress exhibited by the majority of nanocrystalline (*nc*) or ultrafine-grained (*ufg*) materials is accompanied by a dramatic decrease of the ductility or strain to rupture [6,7]. At the early stage of plastic deformation, the stress–strain curves exhibit a rapid and brief hardening for *nc* and *ufg* materials contrariwise to the progressive and higher strain-hardening rate (*shr*) of the coarse-grained counterparts. Furthermore, during straining, a transition from homogeneous deformation with pronounced hardening to localized deformation after the onset of yielding is observed. This behavior appears to be material-structure and deformation-mode independent [6,8].

It has been recently reported in a number of studies that the presence of a large volume fraction of nanoscale twins enhances mechanical characteristics of ultrafine-grained metallic materials [9–12]. This was ascribed to the particular behavior of the twin boundaries (TBs) in accommodating the deformation [9,13]. In the same line, nanoscale lamellar structures in Co–Cu alloys processed by electrodeposition were found to enhance mechanical properties [14], as these boundaries may act the same way as coherent boundaries [15]. The improved mechanical properties of the microstructures having high concentration of planar faults induce a great interest in these materials. At the same time, the deformation mechanisms in the highly faulted materials are not well understood. In the present paper, we study the relationship between the microstructure and the mechanical properties of a highly faulted ultrafine-grained bulk Co processed by powder metallurgy. The underlying deformation mechanisms in compression test at room temperature are established from the change of microstructure during plastic deformation.

2. Experimental procedures

Nanostructured Co particles having an average crystallite size of about 10 nm were synthesized by polyol reduction in 1,2-propanediol [16,17]. The principle is

* Corresponding author. Tel.: +33 1 49403488.
E-mail address: dirras@univ-paris13.fr (G. Dirras).

0925-8388/$ – see front matter © 2009 Elsevier B.V. All rights reserved.
doi:10.1016/j.jallcom.2009.09.153

based on reducing a cobalt salt (0.08 mol/L), with the desired amount of NaOH, in the polyol medium heated up to the boiling point (186 °C). To trigger a heterogeneous nucleation that yields particles with sub-micrometer size, silver nitrate (0.04×10^{-3} mol/L) was added to the precursor. In the final product, the particles were agglomerated into 200 nm sized and high purity Co (>99.99%) clusters containing 85% face-centered cubic (*fcc*) phase and 15% hexagonal close-packed (*hcp*) phase as revealed by X-ray diffraction (XRD) experiments.

Bulk samples were processed from the Co particles by hot isostatic pressing (HIP) [18]. During the HIP-processing, the capsule containing the powder was subjected to a pressure of 200 MPa at 500 °C for 120 min. This resulted in samples having a random crystallographic texture and a mean grain size of 310 ± 20 nm. The particle size in the precursor and the grain size of the bulk samples were measured from transmission electron microscopy micrographs by counting at least 150 particles or grains.

After consolidation, prismatic specimens were cut out from the as-processed bulk samples for uniaxial compression tests as other mechanical investigations should be excluded due to the relatively high porosity of the consolidated samples. Specimens with final dimensions of about 3 mm × 3 mm × 5 mm were prepared and compressed at room temperature and at a strain rate of $\sim 2 \times 10^{-4}\ s^{-1}$.

X-ray diffraction study of the crystalline phase composition was conducted using a Philips Xpert powder diffractometer with CuKα radiation. Specimens for electron microscopy investigations were first mechanically grinded down to a thickness of 50 μm and subsequently thinned using a dimple grinder and finished to perforation using a Gatan™ Precision Ion Polishing System (PIPS). Conventional and high-resolution transmission electron microscopy (CTEM and HRTEM) investigations were conducted on JEOL 2011 and Tecnai FEI electron microscopes, respectively, operating at 200 kV.

3. Results and discussion

The CTEM micrograph displayed in Fig. 1a shows a highly faulted nanoscale lamellar microstructure. Indeed, grains were populated by a high density of plates having thickness in the range of 5–10 nm or less and stacking faults, consistent with the low stacking fault energy of Co. Dislocation contrasts can also be seen, particularly in those grains where the lamellar structure is out of contrast (see the arrows). In addition, voids are also found within the microstructure, probably as a consequence of incomplete particle bonding during sintering. The residual porosity has been estimated from the following expression:

$$p = \left(1 - \frac{\rho_m}{\rho_t}\right) \times 100, \quad (1)$$

where ρ_m is the measured density (in our case ρ_m was determined by Archimede's principle) and ρ_t is the theoritical density of Co. Substituting $\rho_m = 8.13\ g\,cm^{-3}$ and $\rho_t = 8.90\ g\,cm^{-3}$, one obtains $p \sim 9.5\%$. The influence of such a relatively high amount of porosity on the elastic behavior will be discussed.

In Fig. 1b a selected area of a grain having the nanoscale lamellar structure is presented along with the corresponding diffraction pattern with strong streaks. After indexing, it was found that the microstructure consists of an intricate {1 1 1} *fcc* twins coexisting with *hcp* domains. Therefore, in accordance with Nakano et al. [15], the boundaries of the lamellar structure are of *fcc*/*fcc* TBs and *fcc*/*hcp* interphases. The lamellar microstructure is most probably induced by the HIP operation. It was found that the higher the porosity amount (due to incomplete particle bonding) in the consolidated samples, the lower the degree of lamellar structure formation. Therefore, the plastic deformation in the particles during HIP at high temperature resulted in the formation of the lamellar structure, which probably occurs by means of slipping of partial dislocations on every second close-packed planes.

Fig. 2a shows a low magnification HRTEM view of the lamellar structure. The high faulting tendency that results in the observed lamellar structure is clearly evidenced. The letters in Fig. 2b illustrates the packing sequence of the close-packed planes. The observed sequence of planes indicates an intricate microstructure consisting of two unfaulted *hcp* phases (I and III) and one faulted *fcc* phase (II). The black lines indicate the stacking faults in the *fcc* structure and the arrows indicate the boundaries between the phases. It

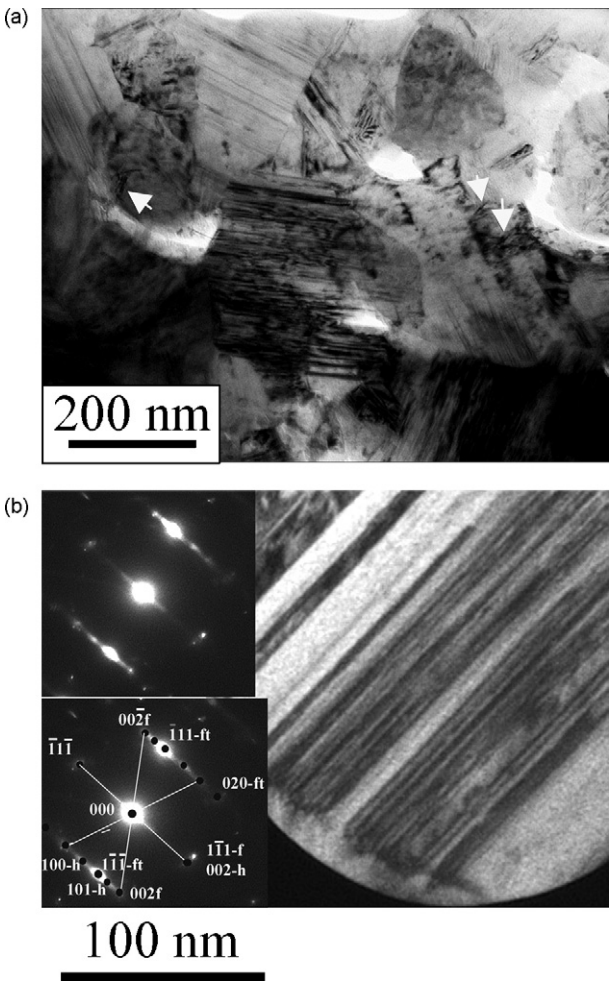

Fig. 1. CTEM micrographs of the microstructure of the as-HIPed samples: (a) a general view showing a layered microstructure and some individual dislocation contrasts (white arrows) and (b) a selected area diffraction pattern of a grain showing spots belonging to *fcc* structure (f), *hcp* structure (h) and fcc twins (ft).

should be noted that other possible division of this plane sequence into *fcc* and *hcp* phases can be also proposed.

Such nanoscale lamellar structures have been reported in electrodeposited (ED) Co [12] where the lamellar structure has been considered as twins, but with no further details provided. Recently, the same kind of nanoscale structures has been developed in electrodeposited Co–Cu alloys [14,15]. Annealing such a microstructure at 973 K resulted in the increase of the width of the *hcp* phase, which was accompanied by a decrease of the stacking disorder and the *fcc*/*hcp* boundaries became coherent [15]. Therefore, these boundaries should possibly act like coherent TBs in enhancing mechanical properties. Actually, there are evidences that TBs may absorb or emit dislocations [19,20] or dislocations can cut them [13] resulting in enhanced mechanical properties. For example, in ultrafine-grained Cu (500 nm) a tremendous increase of the strain rate sensitivity parameter, *m* of the flow stress has been measured in samples containing a high density of twins (width ~20 nm) compared to a twin free sample with the same average grain size. A sustained ductility was then observed upon tensile tests [10].

Fig. 3 shows the mechanical behavior of the as-processed Co sample during compression tests at RT at a strain rate of $\sim 2 \times 10^{-4}\ s^{-1}$ conducted on two specimens from the same bulk sample. The two curves perfectly superimposed despite the fact that one of the specimens failed after a plastic strain of about 2%

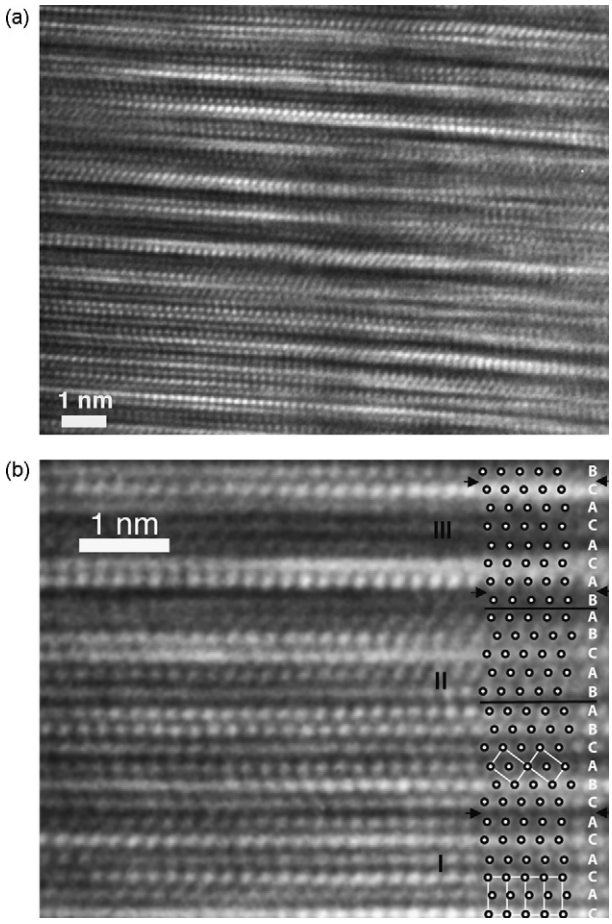

Fig. 2. HRTEM investigations illustrating the highly faulted microstructure: (a) overall view at a lower magnification and (b) details of stacking sequence showing the microstructure consisting of two unfaulted *hcp* phases (I and III) and one faulted *fcc* phase (II). The letters in (b) show the packing sequence of the close-packed planes. The black lines indicate the stacking faults in the *fcc* structure and the arrows indicate the boundaries between the phases. It should be noted that other possible division of this plane sequence into *fcc* and *hcp* phases can be also proposed.

(curve (b) in Fig. 3), probably due to microstructure heterogeneity within the compact as reported elsewhere [21].

The elastic part of the curves allowed computing the Young's modulus value of about 135 ± 5 GPa (also confirmed by nanoindentation test). Such a low value has to be related to the amount of porosity determined above. Using a relation given by Meyers et al.

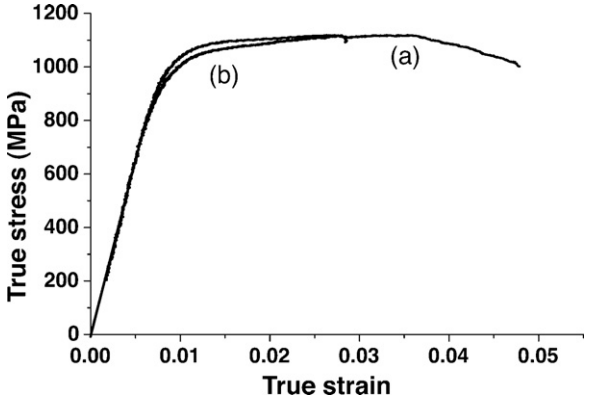

Fig. 3. The room temperature mechanical behavior during compression tests at a strain rate of $\dot{\varepsilon} = 2 \times 10^{-4}\,s^{-1}$ for two specimens cut from the same consolidated disk. See the text for more details.

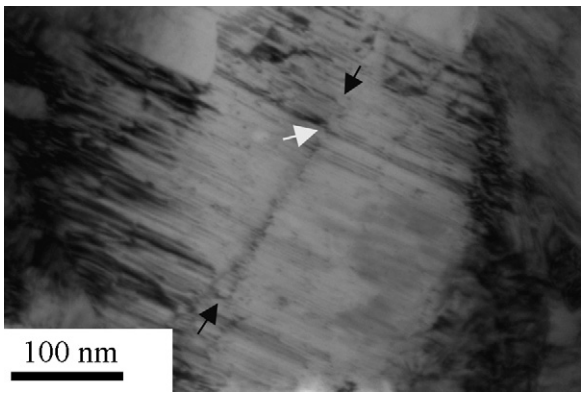

Fig. 4. A CTEM micrograph showing the microstructure after room temperature deformation at a strain of ~3.5%. The black arrows show a dislocation boundary crossing the lamellar structure which induces local shear effect as indicated by the white arrow.

[22], the Young modulus depends on the porosity p as:

$$E = E_0(1 - f_1 p + f_2 p^2) \quad (2)$$

where the constants f_1 and f_2 are equal to 1.9 and 0.9, respectively, and E_0 is the Young's modulus of the fully dense material, equal to ~211 GPa for Co. Substituting these values in Eq. (2), $E = 170$ MPa is computed, which is close to the value obtained from the stress–strain curve (it should be noticed that the strain during compression test was calculated from the crosshead displacement corrected by the stiffness of the testing machine).

It was found that after the onset of yielding, the flow stress increased regularly up to a strain value of about $\varepsilon = 3.5\%$, afterwards the load drops until failure, which occurred at $\varepsilon_r \sim 5\%$ (sample (a)). The proof stress at $\varepsilon = 0.2\%$ and the ultimate strength are $\sigma_{0.2\%} \sim 1000$ MPa and $\sigma_u \sim 1150$ MPa, respectively. The proof stress value is far higher than that predicted by a simple extrapolation of HPL. Indeed, both values of $\sigma_{0.2\%}$ and ε_r compare fairly well with those reported for tensile-tested 12 nm grain-sized *hcp* Co specimens ($\sigma_{0.2\%} \sim 1002$ MPa) [12] but the strength values are lower than those reported for 3 nm sized lamellar domains in Co–Cu alloys ($\sigma_{0.2\%} \sim 1420$ MPa and $\sigma_u \sim 1875$ MPa) [14]. Such a behavior has been attributed to a strengthening effect of the boundaries in the lamellar microstructure, which is similar to the effect of general grain boundaries or coherent TBs, in accordance with [15]. Therefore, in accordance to these previous studies, it can be concluded that the strength of these lamellar microstructures is controlled rather by the lamellae thickness than by the grain size.

In addition, strain rate jump test from $\sim 2 \times 10^{-4}\,s^{-1}$ to $\sim 2 \times 10^{-2}\,s^{-1}$ at $\varepsilon = 1.3\%$ was carried out and allowed to compute the thermal activation parameters which are the strain rate sensitivity parameter of the flow stress, $m \sim 0.014$, and the apparent activation volume $V_a \sim 3b^3$. This value of the activation volume is in accordance with that reported in [14], which was related to dislocation emission from boundaries of the nanoscale lamellar structure due to local stress concentration. Contrariwise, in *hcp* Co it was observed that an increase of the strain rate from $\sim 2 \times 10^{-4}\,s^{-1}$ to $\sim 2 \times 10^{-3}\,s^{-1}$ during tensile tests resulted in softening, also accompanied by a decrease in the total elongation. This behavior was attributed to a deformation mechanism occurring mostly by twinning [12]. In the present case, even if mechanical twinning cannot be ruled out [23], the computed activation volume supports the idea of a deformation mechanism controlled by dislocation emission from the numerous interfaces and their propagation within the lattice. Fig. 4 illustrates the microstructure of a specimen deformed up to about 3.5% plastic strain. Dislocation contrast can hardly be seen but a (low angle) dislocation boundary is observed (aligned along the

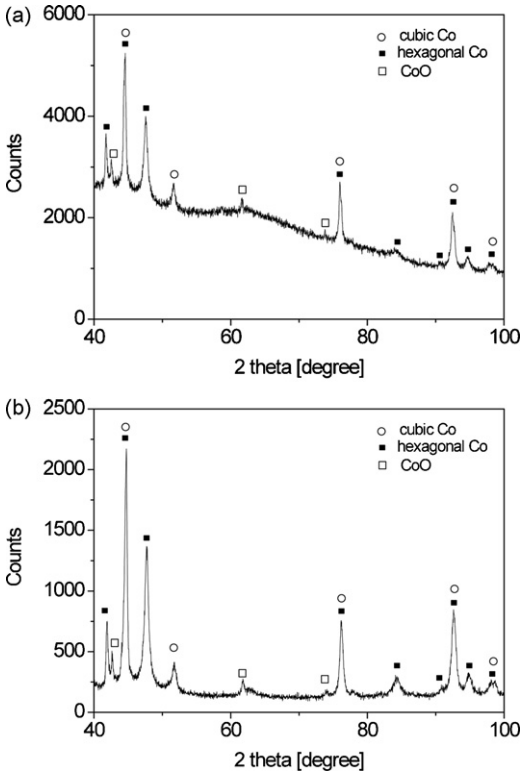

Fig. 5. The X-ray diffractograms obtained before (a) and after (b) straining at RT. See the text for details.

black arrows) interacting with the lamellar structure and resulting in local shear effect (indicated by the white arrow). Such a boundary crossing a lamellar structure has been profusely observed by Wu et al. [24] after surface mechanical attrition of Co.

Nevertheless, a striking feature of the present study is the increasing amount of the *hcp* phase at the expense of *fcc* phase during straining. The phase composition was quantitatively measured by XRD experiments before and after compression test, as it is shown in Fig. 5a and b, respectively. In these investigations, the volume ratio of the different phases was computed by calculating the ratio of the integrated intensities (the area under the peak) of the strongest peaks of the X-ray patterns. For the *hcp* Co phase, this peak is located at $2\theta = 47.5^\circ$. At the same time, the peak having the highest intensity for *fcc* Co strongly overlaps with the *hcp* Co peak at about $2\theta = 44.5^\circ$ and the only peak for *fcc* Co which is free from overlapping is at $2\theta = 51.6^\circ$ with a relative intensity of 40% compared with the strongest peak of *fcc* Co. Therefore, the integrated intensity at the strongest peak for the *fcc* Co phase was estimated from the peak at $2\theta = 51.6^\circ$ multiplied by 2.5. The volume ratio of *fcc* and *hcp* phases was obtained as the ratio of the integrated intensity values of the 100% intensity peaks of the two phases. It was observed that in the undeformed state (Fig. 5a) the fractions of *fcc* and *hcp* phases were 55% and 39%, respectively, and ~6% CoO oxide phase with a *fcc* structure was also observed. After compression (Fig. 5b), the fraction of the *hcp* phase increased to ~65% (29% *fcc*, and 6% CoO). Therefore, the *hcp*/*fcc* amount ratio increased from 1.4 to 2.2. It is thus suggested that the underlying deformation mechanism is mainly based on Shockley partials emission and gliding, that induces the *fcc* to *hcp* phase transformation [25]. Indeed, the gliding process of a Shockley partial dislocation on a close-packed plane was discussed by Jiang et al., in their molecular dynamics study of a martensitic transformation in Co [26]. It has been observed that the atoms swept across by the dislocation line contribute to a displacement close to the Burgers vector of a Shockley dislocation, leading to the production of a new stacking sequence and an *hcp* lamella grows in the *fcc* structure. A similar gliding process has been observed in the case where an intrinsic stacking fault is preexisting in the *fcc* structure. Most probably the same processes likely occurred here.

Recently, Lu et al. [27] have investigated the maximum strength of nanotwinned copper samples with different twin thicknesses. The authors have found that the strongest samples have a twin thickness of 15 nm, and that below this size, softening occurs accompanied by enhanced strain hardening and ductility. In the light of the discussion conducted in [27], we hypothesize that, in our study, the increase of amount of the *hcp* phase during straining is accompanied by a transformation-induced plasticity and also the formation of additional coherent *fcc*/*hcp* interfaces as suggested in [15]. This may lead to a higher flow stress and hardening capability, coupled with a sustainable ductility. Finally, in the deformation mode considered here, the influence of the porosity on the plastic behavior appears to be very remote compared to the effect induced by the lamellar microstructure.

4. Conclusions

Bulk *ufg* Co samples have been processed by HIP from nanopowders synthesized by *chimie douce*. The as-processed material has an intricate *fcc*/*hcp* lamellar microstructure, having enhanced mechanical characteristics during compression test at RT, despite the high porosity level compared with near fully dense materials processed by other methods.

The most important features of the mechanical behavior of this material are:

(i) One of the underlying deformation mechanisms is the lamellar boundary-induced plasticity controlled by dislocations nucleated at these boundaries.
(ii) The *hcp*/*fcc* phase ratio increased during compression test most probably due to the glide of Shockley partials on {1 1 1} planes which also contributes to plastic deformation.
(iii) The mechanical properties also affected by the slip transfer properties at the *fcc*/*hcp* interphase boundaries within the lamellar structure.
(iv) The residual porosity has a significant negative impact on the elastic properties, but not on the overall plastic behavior during compression.

Acknowledgments

This work was conducted in the framework of an interdisciplinary research program at LPMTM. JG is grateful for the support of a Bolyai Janos Research Scholarship of the Hungarian Academy of Sciences.

References

[1] E.O. Hall, Proc. Phys. Soc. Lond. B 64 (1951) 747.
[2] N.J. Petch, J. Iron Steel Inst. 174 (1953) 25.
[3] F. Ebrahimi, G.R. Bourne, M.S. Kelly, T.E.J. Matthews, Nanostruct. Mater. 11 (1999) 343.
[4] C. Cheung, F. Djuanda, U. Erb, G. Palumbo, Nanostruct. Mater. 5 (1995) 513.
[5] J. Schiøtz, K.W. Jacobsen, Science 301 (2003) 1357.
[6] W.Q. Cao, G.F. Dirras, M. Benyoucef, B.J. Bacroix, Mater. Sci. Eng. A 462 (2007) 100.
[7] D. Jia, K.T. Ramesh, E. Ma, Acta Mater. 51 (2003) 3495.
[8] C.Y. Yu, P.W. Kao, C.P. Chang, Acta Mater. 53 (2005) 4019.
[9] M. Dao, L. Lu, Y.F. Shen, S. Suresh, Acta Mater. 54 (2006) 5421.
[10] L. Lu, R. Schwaiger, Z.W. Shan, M. Dao, K. Lu, S.J. Suresh, Acta Mater. 53 (2005) 2169.
[11] L. Lu, Y. Shen, X. Chen, L. Qian, K. Lu, Science 304 (2004) 422.
[12] A.A. Karimpoor, U. Erb, K.T. Aust, G. Palumbo, Scripta Mater. 49 (2003) 651.

[13] Z.H. Jin, P. Gumbsch, E. Ma, K. Albe, K. Lu, H. Hahn, H. Gleiter, Scripta Mater. 54 (2006) 1163.
[14] Y. Nakamoto, M. Yuasa, Y. Chen, H. Kusuda, M. Mabuchi, Scripta Mater. 58 (2008) 731.
[15] H. Nakano, M. Yuasa, M. Mabuchi, Scripta Mater. 61 (2009) 371.
[16] G. Viau, P. Toneguzzo, A. Pierrard, O. Acher, F. Fiévet-Vincent, F. Fiévet, Scripta Mater. 44 (2001) 2263.
[17] F. Fellah, F. Schoenstein, G. Dirras, N. Jouini, in: S.J. Mashl (Ed.), International Conference Hot Isostatic Pressing, Huntington Beach, CA, 2008, pp. 97–104.
[18] S. Billard, J.P. Fondere, B. Bacroix, G.F. Dirras, Acta Mater. 54 (2006) 411.
[19] A. Frøseth, H. Van Swygenhoven, P.M. Derlet, Acta Mater. 52 (2004) 2259.
[20] A.G. Frøseth, P.M. Derlet, H. Van Swygenhoven, Scripta Mater. 54 (2006) 477.
[21] G. Dirras, S. Bouvier, J. Gubicza, B. Hasni, T. Szilàgyi, Mater. Sci. Eng. A 526 (2009) 201.
[22] M.A. Meyers, A. Mishra, D.J. Benson, Prog. Mater. Sci. 51 (2006) 427.
[23] X. Wu, N. Tao, Y. Hong, J. Lu, K. Lu, Scripta Mater. 52 (2005) 547.
[24] X. Wu, N. Tao, Y. Hong, G. Liu, B. Xu, J. Lu, K. Lu, Acta Mater. 53 (2005) 681.
[25] D.W. Bray, J.M. Howe, Metall. Mater. Trans. 27a (1996) 3362.
[26] M. Jiang, K. Oikkawa, T. Ikeshoji, Metall. Mater. Trans. 36a (2005) 2307.
[27] L. Lu, X. Chen, X. Huang, K. Lu, Science 323 (2009) 607.